Journal of Power Sources 196 (2011) 2227–2240

Contents lists available at ScienceDirect

Journal of Power Sources

journal homepage: www.elsevier.com/locate/jpowsour

Discrimination of Li-ion batteries based on Hamming network using discharging–charging voltage pattern recognition for improved state-of-charge estimation

Jonghoon Kim*, Seongjun Lee, B.H. Cho

Power Electronics System Laboratory, School of Electrical Engineering and Computer Science, Seoul National University, Seoul 151-744, Republic of Korea

ARTICLE INFO

Article history:
Received 3 June 2010
Received in revised form 19 August 2010
Accepted 26 August 2010
Available online 25 October 2010

Keywords:
Hamming network
Pattern recognition
State-of-charge (SoC)
Lumped parameter battery model
Li-ion battery

ABSTRACT

Differences in electrochemical characteristics among Li-ion batteries and factors such as temperature and ageing result in erroneous state-of-charge (SoC) estimation when using the existing extended Kalman filter (EKF) algorithm. This study presents an application of the Hamming neural network to the identification of suitable battery model parameters for improved SoC estimation. The discharging–charging voltage (DCV) patterns of ten fresh Li-ion batteries are measured, together with the battery parameters, as representative patterns. Through statistical analysis, the Hamming network is applied for identification of the representative DCV pattern that matches most closely of the pattern of the arbitrary battery to be measured. Model parameters of the representative battery are then applied to estimate the SoC of the arbitrary battery using the EKF. This avoids the need for repeated parameter measurement. Using model parameters selected by the proposed method, all SoC estimates (off-line and on-line) based on the EKF are within ±5% of the values estimated by ampere-hour counting.

1. Introduction

The Li-ion battery is widely used in many fields because of its advantages of high voltage, low mass, low self-discharge, and long cycle-life. High specific energy, in particular, makes it a promising candidate for electric vehicles (EVs) and hybrid electric vehicles (HEVs) [1–3]. In such applications, a battery management system (BMS) is critical for maintaining optimum battery performance, and the most important parameter controlled by such a system is the state-of-charge (SoC) [4,5]. Precise SoC information is critical in practical applications where it is necessary to determine how long the battery will last and, importantly, when to stop charging and discharging, as over-charging and over-discharging may cause permanent internal damage.

In recent years, much research has been devoted to developing improved methods for SoC estimation [6–10]. Ampere-hour counting, the most common method, is easy and reliable, but can suffer from initial value errors and accumulated errors from incorrect measurements, in addition to inherent inaccuracy stemming from unaccounted current losses. The open-circuit voltage (OCV) method is very accurate, but cannot be used in real time as the battery must first be disconnected. These drawbacks with conventional methods are addressed by new adaptive methods that rely on computational techniques such as neural networks, fuzzy logic, adaptive observers, and the extended Kalman filter (EKF). The EKF method, in particular, has seen substantial progress in recent years [11–13]. This method is known to be an optimum adaptive algorithm based on recursive estimation. The accuracy of the EKF depends largely on predetermined parameter values used in the lumped parameter model of the battery system. As shown in Fig. 1, it is very important to measure correctly model parameters that include the OCV, series resistance (R_i), diffusion resistance (R_{Diff}), and diffusion capacitance (C_{Diff}) [14–18]. Since, however, these parameters vary with electrochemical characteristics [19–21], temperature [22–31] and age [32–41], the accuracy of this estimation method will also vary. The error can be reduced by repeated measurement of parameter values, but such an exercise would be very time-consuming and inefficient. Thus, existing EKF algorithms can only be applied to a single battery under controlled experimental conditions [15–18].

In general, battery voltage changes with the discharging/charging pulse current. In addition, the magnitude of the increase or decrease in this voltage, called the voltage variance, is associated with changes in battery parameters. That is, the voltage variance can be used to determine the magnitude of the parameters for the battery model (Fig. 1). For reference, two resistances, namely, the series resistance (R_i) and the diffusion resistance (R_{Diff}), are considered critical factors. When a constant discharg-

* Corresponding author. Tel.: +82 2 880 1785; fax: +82 2 878 1452.
E-mail address: qwzxas@hanmail.net (J. Kim).

0378-7753/$ – see front matter © 2010 Elsevier B.V. All rights reserved.
doi:10.1016/j.jpowsour.2010.08.119

Nomenclature

SoC	state-of-charge
EKF	extended Kalman filter
OCV	open circuit voltage
Ri	series resistance
R_{Diff}	diffusion resistance
C_{Diff}	diffusion capacitance
DCV	discharging/charging voltage
DV	discharging voltage
CV	charging voltage
DCIR	direct current internal resistance
K_k	Kalman gain
x_k	state
w_k	process noise
Q_k	process noise covariance
v_k	measurement noise
R_k	measurement noise covariance
P_k	covariance matrix of state estimation uncertainty
H_k	measurement sensitivity matrix
HD	Hamming distance
W	weight matrix
b	bias vector
p	input vector
a	output vector
R	number of elements in each input vector
S	number of neurons
ε	lateral interaction coefficient
ISVP	initial starting voltages points
m	average of each characteristic parameter
std	standard deviation of each characteristic parameter
α	tuning value

ing/charging current is commonly applied to the batteries, the magnitudes of the respective voltage variances are different. In addition, the discharging/charging voltage (DCV) pattern of each battery is almost constant under identical conditions such as voltage magnitude, current type (discharging/charging), and time interval. Therefore, the DCV pattern can be used to discriminate among Li-ion batteries with different characteristics for improved SoC estimation. This investigation proposes the use of a Hamming neural network for such DCV pattern recognition. The Hamming network is generally used and designed explicitly for binary pattern recognition. In this study, the Hamming network is used to evaluate several predetermined representative DCV patterns and determine the one that is closest to the input DCV pattern by comparing the inner products. Through statistical analysis, the proposed method can perform recognition of an arbitrary DCV pattern. Representative DCV patterns are collected from ten fresh Li-ion batteries,

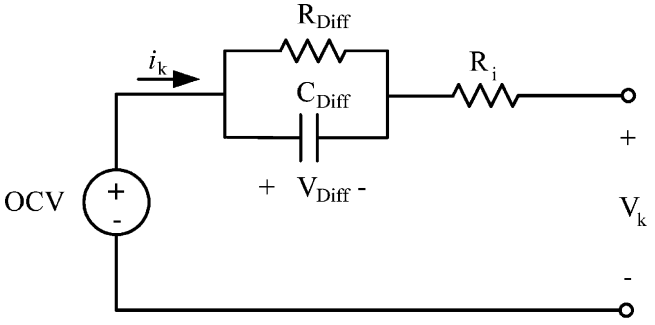

Fig. 1. Lumped parameter battery model: open-circuit voltage (OCV), series resistance (R_i), diffusion resistance (R_{Diff}), and diffusion capacitance (C_{Diff}).

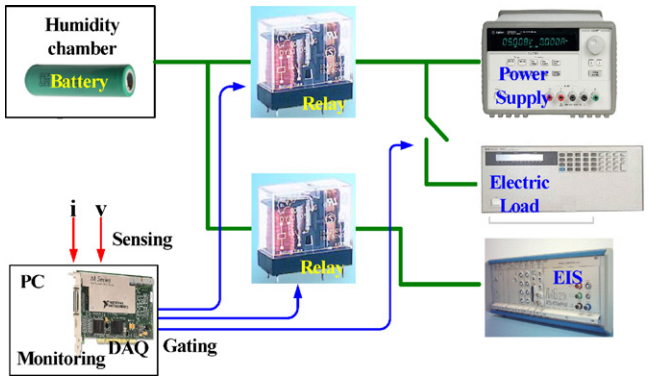

Fig. 2. Experimental setup.

together with seven characteristic model parameters for each battery. In addition, to simplify the statistical analysis, all the DCV patterns are separated into two groups: discharging voltage (DV) patterns and charging voltage (CV) patterns. Finally, the model parameters of the identified representative battery are used for SoC estimation of an arbitrary battery. This avoids the need for repeated measurement of model parameters. The SoC estimates based on off-line and on-line methods are compared with those of ampere-hour counting. Then, two SoC estimation results of the EKF satisfy the specification within ±5%.

2. Experimental

Experimental studies were conducted on Samsung 18650 Li-ion batteries that had a rated capacity of 1.3 Ah. As shown in Fig. 2, the experimental set-up comprised a power supply for battery charging (Agilent E3633A), an electric load for discharging (Hewlett Packard 6050A), a humidifier chamber for temperature control (Hitachi U-6652P-CH3), and an electrochemical impedance spectroscope (EIS) for obtaining impedance plots (Zahner IM6ex). The experimental results were collected with a data-acquisition board, stored on a PC, and used as inputs for MATLAB/Simulink S-function simulations. All experiments were performed at 25 °C.

For reference, the rated capacity was measured by fully charging–discharging scheme. For fully charging Li-ion batteries, the constant current–constant-voltage (CC–CV) protocol was used. A direct current of 0.65 A(C/2) was used to charge the battery during the constant current part and the cut-off voltage was set at 4.2 V. Subsequently, the voltage was held constant at 4.2 V till the current fell to 100 mA. After fully charging, the constant-current (CC) protocol was used for fully discharging. A direct current of 4 A(3C) was used to discharge the battery and the cut-off voltage was set at 2.8 V. Using this protocol, the battery could be completely discharged to obtain the capacity. So, the batteries were operated within the voltage range from 2.8 V to 4.2 V.

In the entire SoC range at each 10% SoC interval (except at SoC 0% and 100%), the OCV, the direct current internal resistance (DCIR) [42] and the impedance were measured by a 10% SoC CC discharging segment. During a period of 1 h, the interval between the previous discharging and the following discharging, a rest period was applied to return to the electrochemical and thermal equilibrium conditions. The battery voltage was stable during the experiments and changed by <1 mV. The impedance data generally covered a frequency range of 1 mHz to 100 kHz in the potentiostatic mode. A sinusoidal a.c. voltage signal of ±5 mV was applied.

3. Battery parameters and a.c. impedance measurements

The model parameters and a.c. impedance were measured to determine their variance with electrochemical characteristics and

Table 1
Rated capacities (Ah) of ten fresh Li-ion batteries at 25 °C.

Battery	No. 1	No. 2	No. 3	No. 4	No. 5
Capacity [Ah]	1.2748	1.2844	1.2826	1.2841	1.2865
Battery	No. 6	No. 7	No. 8	No. 9	No. 10
Capacity [Ah]	1.2761	1.2925	1.2753	1.2704	1.2796

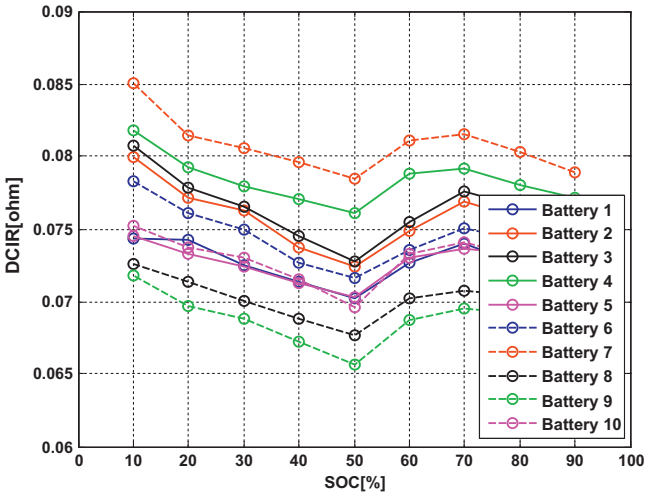

Fig. 3. DCIR ($R_i + R_{Diff}$) results for ten fresh batteries at 25 °C.

temperature/ageing effects. Note that in exploring the question of parameter variation, this paper is limited to two resistances—series resistance (R_i) and diffusion resistance (R_{Diff}).

3.1. Electrochemical characteristics

Model parameters are not always consistent across batteries with similar rated capacities. Table 1 shows the rated capacities of ten fresh Li-ion batteries. As shown in Fig. 3, in the entire SoC range except at SoC 0% and 100%, the sum of two resistances ($R_i + R_{Diff}$), called DCIR, is not consistent. In addition, the inconsistent DCIR values are shown at SoC 60% for the ten experimental batteries.

3.2. Temperature and ageing effects

Model parameters generally vary with temperature. The DCIR and R_{Diff} of ten fresh batteries at various temperatures (10–50 °C) at SoC 60% are compared with those at 25 °C in Fig. 4. Due to the different electrochemical characteristics, large differences are seen in the DCIR and R_{Diff} results among the batteries. Fig. 5 shows a.c. impedance measurements made using Nyquist plots in the frequency domain at SoC 30, 60, and 90%. It is seen that temperature has a significant effect on the a.c. impedance. With increased temperature, the diameter of the two overlapping arcs, which reflects the R_{Diff} becomes smaller. Consequently, it can be concluded that R_{Diff} is the primary factor affected by temperature.

Ageing is another important effect that influences battery parameters. Calendar-life tests [43] were used to degrade performance over periods of 50–150 days at 60 °C. The a.c. impedance measurements of aged batteries using Nyquist plots in the frequency domain at SoC 30 and 60% at 25 °C are presented in Fig. 6. The diameters of the two overlapping arcs are clearly related to ageing time. Thus, R_{Diff} as a primary factor is influenced by ageing. Due to the different electrochemical characteristics, there is some difference between the diameters of the overlapping arcs in the impedance spectra at SoC 30 and 60%. Combined temperature/ageing effects can cause large differences, as shown in Table 2, Figs. 7 and 8. The ageing effect led to the most marked differences in the diameters of the two overlapping arcs from that of a fresh battery.

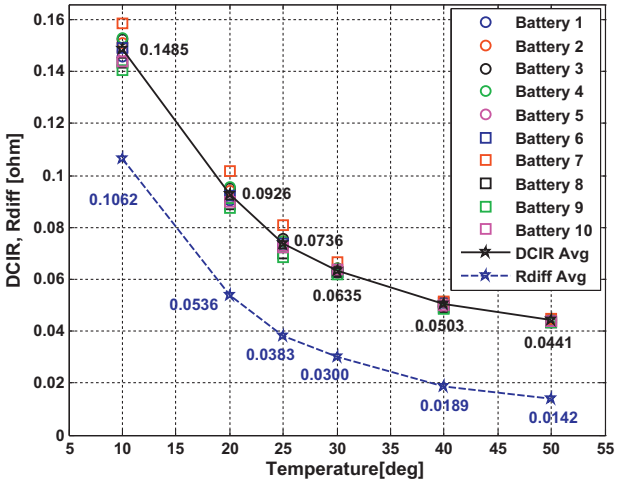

Fig. 4. DCIR and R_{Diff} results for ten fresh batteries at various temperatures (10–50 °C; interval, 10 °C).

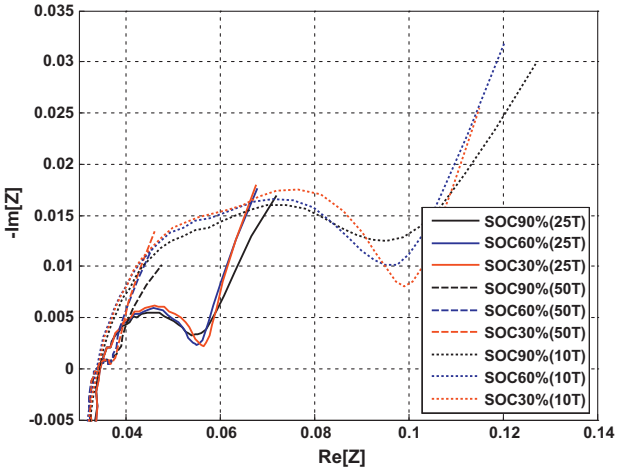

Fig. 5. a.c. impedance spectra of fresh battery at 10, 25 and 50 °C (SoC 30, 60, and 90%).

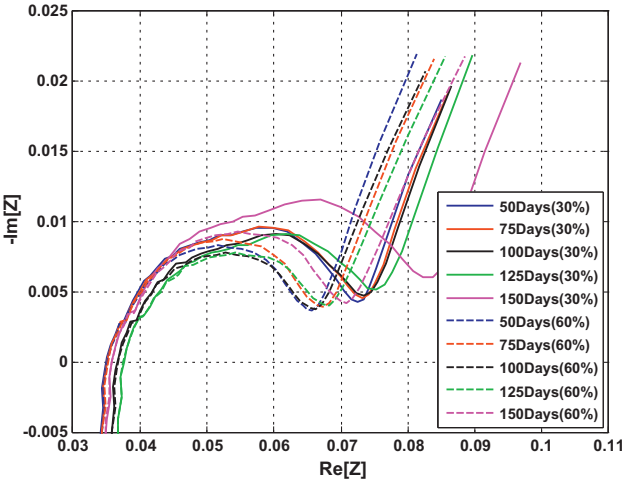

Fig. 6. a.c. impedance spectra of aged batteries at 25 °C (SoC 30 and 60%).

Table 2
Rated capacities (Ah) of fresh battery and five batteries aged at 10, 25 and 50 °C.

Calendar-life test days	Capacity [Ah] 10°C	Capacity [Ah] 25°C	Capacity [Ah] 50°C
No of days (Fresh)	1.1113	1.2901	1.3192
50 days	0.9890	1.1482	1.2352
75 days	0.9622	1.1170	1.1834
100 days	0.9057	1.0515	1.1332
125 days	0.8649	1.0041	1.1039
150 days	0.8577	0.9957	1.0649

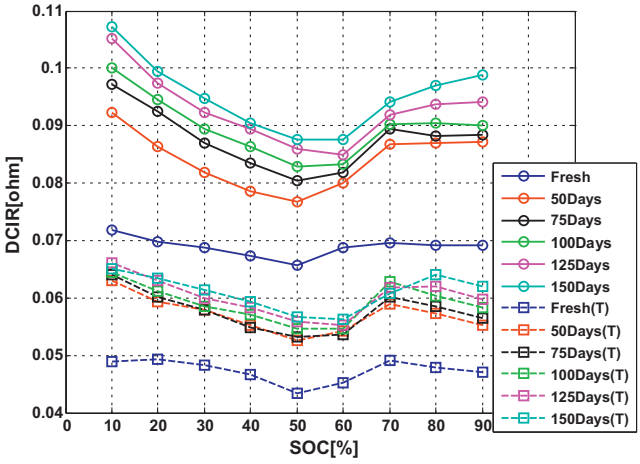

Fig. 7. DCIR ($R_i + R_{Diff}$) results for a fresh battery and aged batteries at 25 and 50 °C.

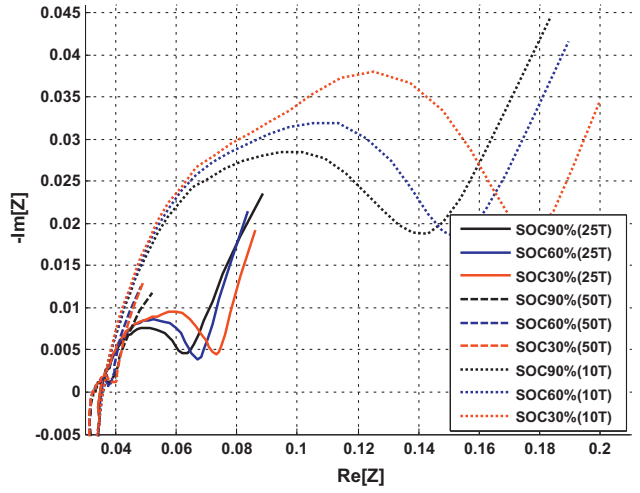

Fig. 8. a.c. impedance spectra of aged batteries at 10, 25 and 50 °C (SoC 30, 60, and 90%).

Consequently, it should be mentioned that model parameters are greatly varied by the three factors. These factors lead to low BMS performance but, to date, no definitive solution exists.

4. Extended Kalman filter (EKF)

The EKF is the optimum state estimator for a non-linear system and is widely used for SoC estimation. In general, the dynamic and measurement models used in the EKF are as follows.

$$\text{Dynamic model}: \quad x_k = f_{k-1}(x_{k-1}) + g(u_{k-1}) + w_{k-1} \quad w_k \sim N(0, Q_k) \tag{1}$$

$$\text{Measurement model}: \quad z_k = h_k(x_k) + i(u_k) + v_k \quad v_k \sim N(0, R_k) \tag{2}$$

Here w_k represents process noise and is assumed to be independent, zero-mean, Gaussian noise with a covariance matrix Q_k. The measurement noise v_k is assumed to be independent, zero-mean, Gaussian noise with a covariance matrix R_k. Then, the equations that decide the Kalman gain K_k are as follows:

$$K_k = P_k H_k^T [H_k P_k H_k^T + R_k]^{-1} \tag{3}$$

$$\hat{x}_k(+) = \hat{x}_k(-) + K_k[Z_k - H_k \hat{x}_k(-)] \tag{4}$$

where the error covariance matrix is P_k and the measurement sensitivity matrix is H_k.

Estimation of the SoC requires a lumped parameter model (Fig. 1) that represents the static and dynamic behaviour of the battery. This can serve to construct the simplified model and prevent the EKF algorithm from measurement errors caused by inaccurate modelling. The simplified model has only two states. With the states incorporated, the dynamic model for the EKF is expressed as:

$$x_k = \begin{bmatrix} \text{SoC} \\ V_{\text{Diff\_}k} \end{bmatrix} = \begin{bmatrix} 1 & 0 \\ 0 & 1 - \dfrac{\Delta t}{C_{\text{Diff}} R_{\text{Diff}}} \end{bmatrix} \begin{bmatrix} \text{SoC}_{k-1} \\ V_{\text{Diff\_}k-1} \end{bmatrix} + \begin{bmatrix} \dfrac{\Delta t}{C_n} \\ \dfrac{\Delta t}{C_{\text{Diff}}} \end{bmatrix} i_{k-1} \tag{5}$$

The measurement model and the terminal voltage of the battery are expressed by the following non-linear function.

$$V_k = h_k(\text{OCV}, V_{\text{Diff}}) - R_i i_k = \text{OCV} - V_{\text{Diff}} - R_i i_k \tag{6}$$

The OCV in the measurement equation is implemented by the OCV–SoC relationship:

$$\frac{\partial h_k}{\partial x_k} = \begin{bmatrix} \dfrac{\partial h_{\text{SoC}}(\text{SoC})}{\partial \text{SoC}} & 0 \\ 0 & -1 \end{bmatrix} \quad \text{OCV} = h_{\text{SoC}}(\text{SoC}), \quad h_{\text{SoC}} = f_{\text{ocv}}^{-1} \tag{7}$$

5. Hamming network

The Hamming neural network [44–50] is used for pattern recognition, as shown in Fig. 9. It is one of the simplest examples of a competitive network and is designed explicitly to solve binary pattern recognition issues. The Hamming network decides which representative pattern is closest to the current pattern by comparing the inner products. Its objective is to decide which prototype vector is closest to the input vector. The Hamming network consists of two layers: the feedforward layer and the recurrent layer.

5.1. Feedforward layer

The feedforward layer calculates a correlation or inner product between each representative pattern and the current pattern in order to find the minimum Hamming distance (HD) from calculation the difference between dimension m and HD. In order to calculate the inner product, a weight matrix $\mathbf{W^1}$ is a set of prototype vectors and is transformed into a binary form, in addition to the bias vector, $\mathbf{b^1}$:

$$\mathbf{W}^1 = \begin{bmatrix} {}_1\mathbf{w}^{iT} \\ {}_2\mathbf{w}^{iT} \\ \vdots \\ {}_S\mathbf{w}^{iT} \end{bmatrix} = \frac{1}{2} \begin{bmatrix} {}_1\mathbf{w}^1 & {}_2\mathbf{w}^1 & \cdots & {}_S\mathbf{w}^1 \\ {}_1\mathbf{w}^2 & {}_2\mathbf{w}^2 & \cdots & {}_S\mathbf{w}^2 \\ \vdots & \vdots & \ddots & \vdots \\ {}_1\mathbf{w}^R & {}_2\mathbf{w}^R & \cdots & {}_S\mathbf{w}^R \end{bmatrix} = \begin{bmatrix} \mathbf{p}_1^T \\ \mathbf{p}_2^T \\ \vdots \\ \mathbf{p}_S^T \end{bmatrix} \tag{8}$$

$$\mathbf{b}^1 = [R, R, \ldots, R] = \left[\frac{m}{2}, \frac{m}{2}, \ldots, \frac{m}{2}\right] \tag{9}$$

where each row of $\mathbf{W^1}$ represents a prototype vector which it is required to be recognize; each element of $\mathbf{b^1}$, $m/2$, is the threshold value and is set equal to the number of elements in each input vector R; and S is the number of neurons. As expressed in Eq. (10), it is high desirable to have the ith ($1 \le i \le R$) node in this layer compute $m - HD({}_i\mathbf{w}, \mathbf{p})$ for a given input vector $\mathbf{p}$, where $HD({}_i\mathbf{w}, \mathbf{p})$ is the Hamming distance between vectors ${}_i\mathbf{w}$ and $\mathbf{p}$. Then, the net input of node is as in Eq. (11), namely, the feedforward layer output. Finally,

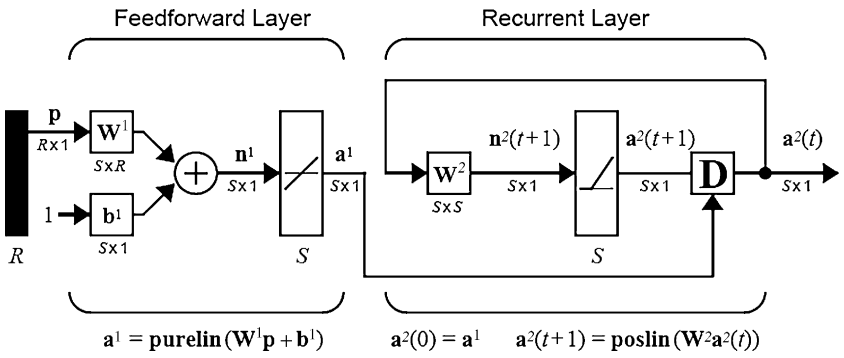

Fig. 9. Hamming network.

these outputs are equal to the inner (Eq. (12)). The neuron in this layer with the largest output corresponds to the prototype pattern that is closest in Hamming distance to the input pattern.

$$\mathbf{W}^1\mathbf{p} = [m - HD({}_i\mathbf{w}, \mathbf{p})] - HD({}_i\mathbf{w}, \mathbf{p}) \tag{10}$$

$$\text{net}_i = \mathbf{n}^1 = \mathbf{W}^1\mathbf{p} + \frac{m}{2} = m - HD({}_i\mathbf{w}, \mathbf{p}) \quad i = 1, 2, \ldots, S \tag{11}$$

$$\mathbf{a}^1 = \mathbf{W}^1\mathbf{p}+\mathbf{b}^1 = \begin{bmatrix} \mathbf{p}_1^T\mathbf{p} + R \\ \mathbf{p}_2^T\mathbf{p} + R \\ \vdots \\ \mathbf{p}_S^T\mathbf{p} + R \end{bmatrix} = \mathbf{purelin}(\mathbf{W}^1\mathbf{p} + \mathbf{b}^1) \tag{12}$$

5.2. Recurrent layer

The recurrent layer is known as the MAXNET. It is a competition layer that performs the winner-take-all (WTA) operation, whose purpose is to enhance the initial dominant response of the *i*th node and suppress the others [50]. The neurons are initialized with the outputs of the feedforward layer, which indicate the correlation between the prototype vectors and the input vector:

$$\mathbf{a}^2(0) = \mathbf{a}^1 \tag{13}$$

As a result of recurrent processing, the *i*th node responds positively, whereas the responses of all remaining nodes decay to zero. Thus, in order to determine a winner (which only has a positive output), the neurons compete with each other. Then, the recurrent layer output is updated according to the following recurrence relation using a positive transfer function (**poslin**):

$$\mathbf{a}^2(t+1) = \mathbf{poslin}(\mathbf{W}^2\mathbf{a}^2(t)) \tag{14}$$

This processing requires self-feedback connections and negative lateral inhibition connections in which the output of each neuron has an inhibitory effect on all of the other neurons. The $n \times n$ weight matrix of the recurrent layer $\mathbf{W^2}$ is taken in Eq. (15). The weights in this layer are set so that the diagonal elements are 1, and the off-diagonal elements have a small negative value, where $0 < \varepsilon < 1/(S-1)$ is called the lateral interaction coefficient. Thus, weight values of 1 and $-\varepsilon$ can be set for the appropriate elements of $\mathbf{W^2}$ in Eq. (16), where $1 \le i \le S$ and $1 \le j \le S$.

$$\mathbf{W}^2 = \begin{bmatrix} \mathbf{w}^1 & \mathbf{w}^2 & \cdots & \mathbf{w}^S \\ \mathbf{w}^1 & \mathbf{w}^2 & \cdots & \mathbf{w}^S \\ \vdots & \vdots & \ddots & \vdots \\ \mathbf{w}^1 & \mathbf{w}^2 & \cdots & \mathbf{w}^S \end{bmatrix} = \begin{bmatrix} 1 & -\varepsilon & \cdots & -\varepsilon \\ -\varepsilon & 1 & \cdots & -\varepsilon \\ \vdots & \vdots & \ddots & \vdots \\ -\varepsilon & -\varepsilon & \cdots & 1 \end{bmatrix} \tag{15}$$

$$\mathbf{a}_i^2(t+1) = \mathbf{poslin}\left(\mathbf{a}_i^2(t) - \varepsilon\sum_{j \neq i}\mathbf{a}_j^2(t)\right) \tag{16}$$

The output of each neuron decreases in proportion to the sum of the outputs of the other neutrons. The output of the neuron with the largest initial output decreases more slowly than the outputs of the other neurons. But eventually, only one neuron will have a positive output. The index of the recurrent layer neuron with a stable positive output is the index of the prototype vector that is the best match with the input.

6. Proposed approach

6.1. Discharging/charging voltage (DCV) measurement

After fully charging (SoC 100%) at a constant current of 4 A, followed by a rest period, each battery was discharged to SoC 80%. Then, for a scaled-down discharging/charging current profile (Fig. 10(a)) of a HEV (time interval, 100 ms), the DCV data collected is shown in Fig. 10(b). The DCV pattern is recognized through experiments for 20 fresh 1.3-Ah Li-ion batteries at 25 °C (Fig. 11).

6.2. Initial starting voltage points (ISVP)

For recognition of the DCV pattern with the Hamming network, statistical analysis is absolutely necessary. First, given current *i*, all DCVs are separated into two patterns: discharging voltage patterns (DV; $i \ge 0$) and charging voltage patterns (CV; $i < 0$), as shown in Fig. 12(a) and (b). Second, the initial starting points of each DV and CV pattern should be fixed. As shown in Figs. 13 and 14, the initial starting voltage points (ISVP) of the ten representative batteries are not fixed due to their different electrochemical characteris-

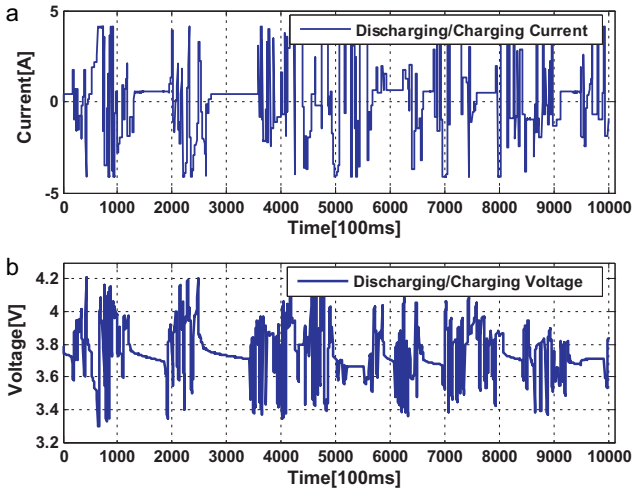

Fig. 10. Two plots for discharging/charging voltage pattern (DCV): (a) current profile; (b) voltage data.

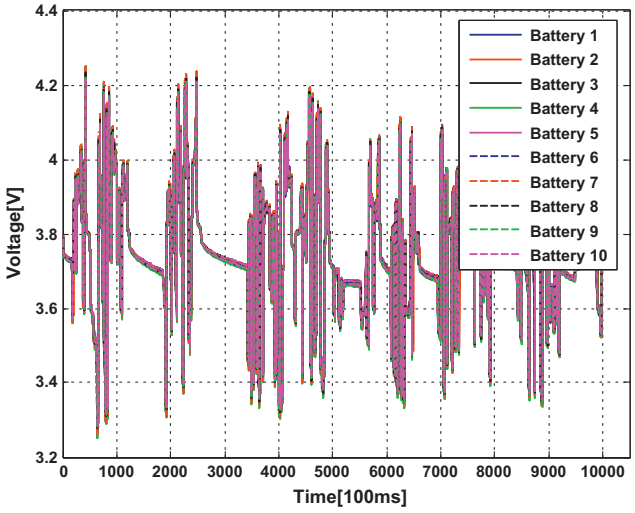

Fig. 11. Discharging/charging voltage patterns for ten Li-ion batteries.

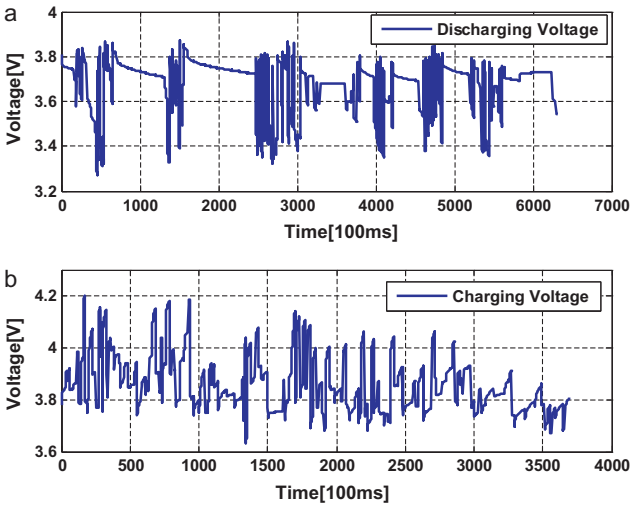

Fig. 12. Two patterns separated from DCV pattern: (a) discharging voltage pattern (DV), (b) charging voltage pattern (CV).

tics. Hence, the average and standard deviations of the collected discharging/charging voltages cannot be compared. Therefore, it is required to set a standard ISVP, as shown in Fig. 15.

Table 3
Characteristics of AVE and STD in relation to voltage variance.

Voltage variance (initial voltage – final voltage)	Discharging		Charging	
	AVE	STD	AVE	STD
Large voltage variance	Small	Large	Large	Large
Small voltage variance	Large	Small	Small	Small

Table 4
Seven characteristic parameters.

DCV pattern	C1	Standard deviation DCV
DV pattern	C2	Standard deviation DV
CV pattern	C3	Standard deviation CV
DV pattern	C4	Average DV ⓕ
	C5	Standard deviation DV ⓕ
CV pattern	C6	Average CV ⓕ
	C7	Standard deviation CV ⓕ

Standard: No. 6 (discharging), No. 1 (charging) ⓕ: fixation

For example, consider three batteries (A–C) with different ISVPs (V_{A11}–V_{C11}). If the standard battery is set as B ($V_{B1I} = V_{B2I}$), then the voltages of A and C are higher and lower, respectively ($V_{A1I} \rightarrow V_{A2I}$; $V_{C1I} \rightarrow V_{C2I}$). Therefore, the three ISVPs are fixed at one point. The fixed discharging/charging voltages are given in Fig. 16(a) and (b), respectively. All average and standard deviations for the collected discharging/charging voltages can be compared by statistical analysis. For given the discharging/charging conditions, the average (AVE) and standard deviation (STD) in relation to voltage variance are presented in Table 3. Regardless of the discharging/charging conditions, the STD values increased at large voltage variance. These features of AVE and STD are used to implement some characteristic parameters of the Hamming network, as shown in Table 4.

6.3. Characteristic parameters of DCV pattern

Here, as indicated in Table 4, seven characteristic parameters (C1–C7) are learned by the Hamming network using the averages and standard deviations based on DCV, DV and CV patterns. Each value of the seven characteristic parameters corresponding to the ten representative DCV patterns is transformed into 1 and −1 array as the four levels of Fig. 17. If these patterns are not transformed into this binary form, then the pattern recognition performance can be distorted by the one parameter that has a large real value. In Fig. 17, *m* is the average and *std* is the standard deviation of each characteristic parameter, and these values are given in Table 5. The levels of each parameter are decided by

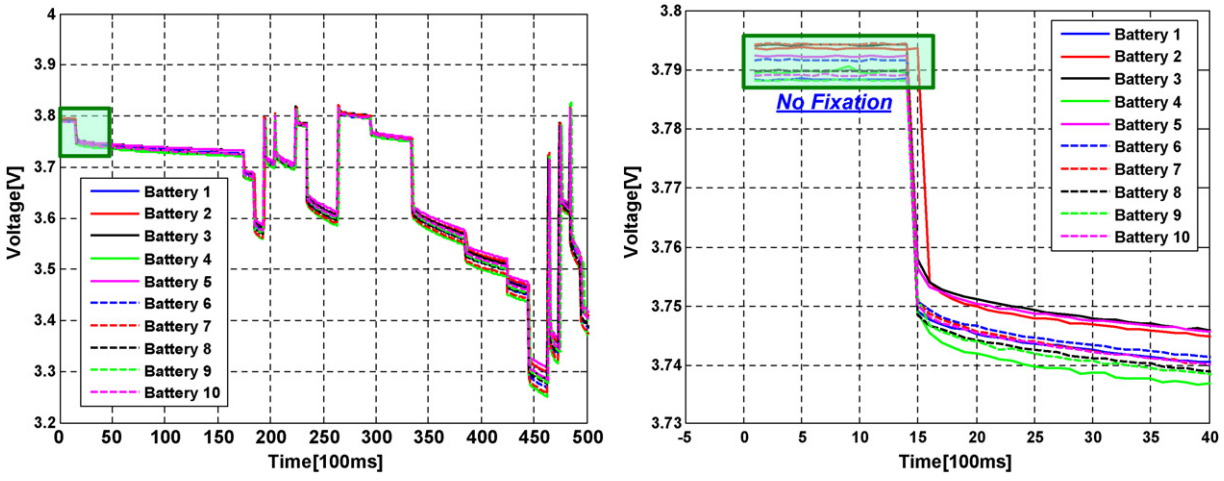

Fig. 13. Unfixed discharging voltages for ten Li-ion batteries.

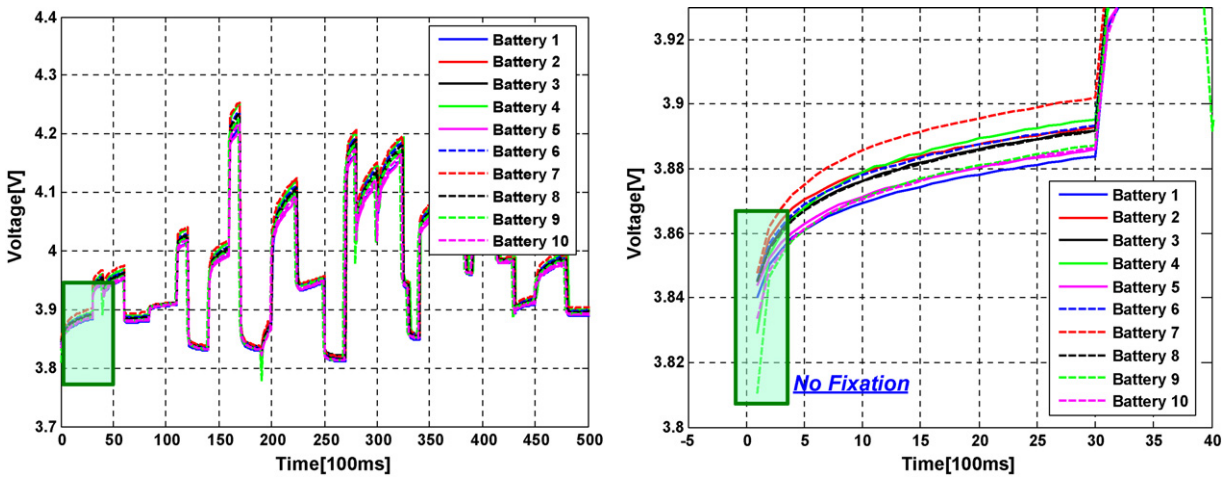

Fig. 14. Unfixed charging voltages for ten Li-ion batteries.

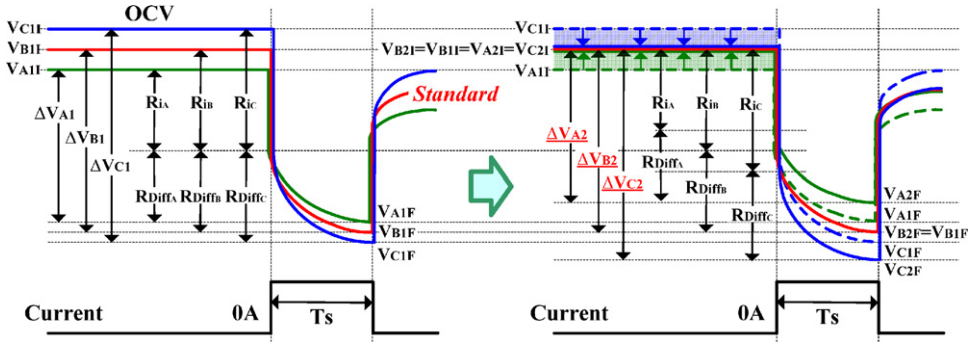

Fig. 15. Initial starting voltage points (ISVP) fixation.

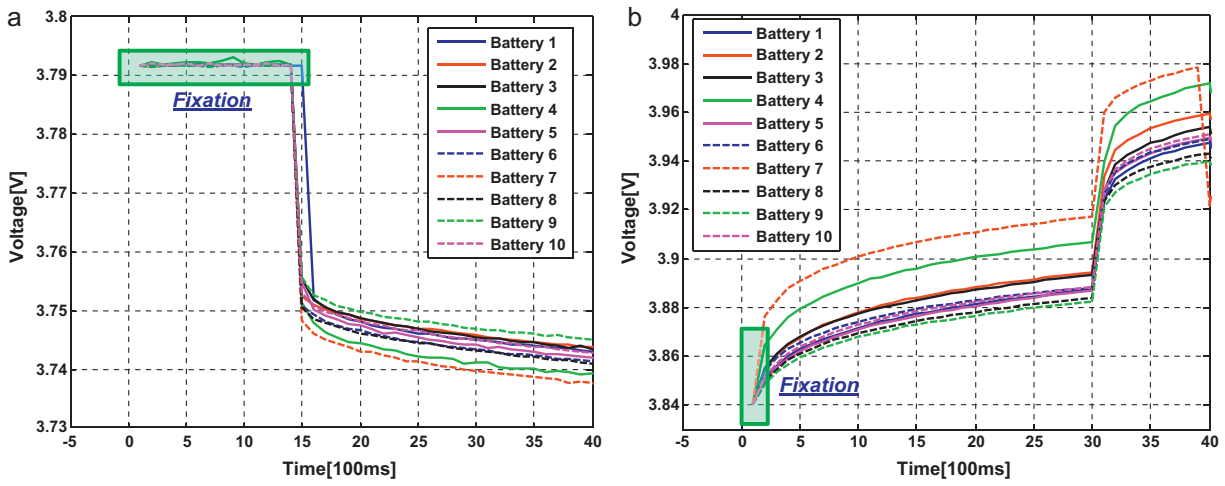

Fig. 16. Fixed discharging/charging voltages of ten Li-ion batteries: (a) discharging; (b) charging.

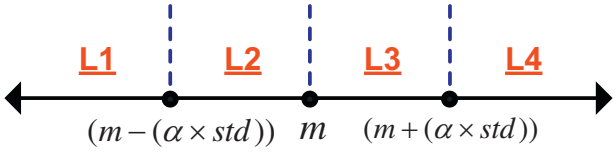

Fig. 17. Four levels and three standards.

three standards, viz., $m-(\alpha \times std)$, m, and $m+(\alpha \times std)$. The levels are decided according to the values of the parameters, as shown in Fig. 18. For example, if the value is larger than $m-(\alpha \times std)$ and smaller than m, the level is L2; α is a tuning value and is chosen as 0.5 to make the characteristic differences of ten representative patterns.

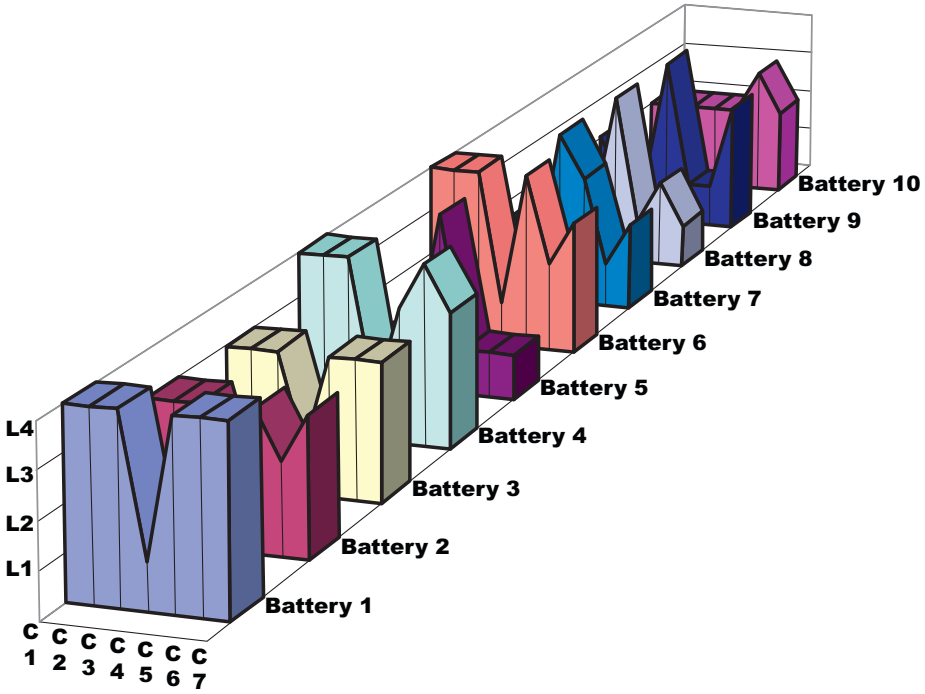

Fig. 18. Characteristics of ten representative patterns.

Table 5
Average (m) and standard deviation (std) of each characteristic parameter.

Battery	C1–C7						
	DCV	DV	CV	DV ⓕ		CV ⓕ	
	Standard	Standard	Standard	Average	Standard	Average	Standard
No. 1	0.1673	0.1199	0.1170	3.6456	0.1201	3.9299	0.1168
No. 2	0.1699	0.1244	0.1212	3.6317	0.1244	3.9345	0.1212
No. 3	0.1710	0.1261	0.1222	3.6289	0.1261	3.9355	0.1222
No. 4	0.1727	0.1263	0.1227	3.6280	0.1263	3.9368	0.1227
No. 5	0.1683	0.1210	0.1179	3.6431	0.1215	3.9321	0.1180
No. 6	0.1693	0.1235	0.1199	3.6332	0.1230	3.9340	0.1192
No. 7	0.1739	0.1276	0.1240	3.6255	0.1276	3.9379	0.1240
No. 8	0.1657	0.1167	0.1135	3.6478	0.1180	3.9242	0.1134
No. 9	0.1637	0.1145	0.1121	3.6503	0.1123	3.9217	0.1112
No. 10	0.1669	0.1193	0.1165	3.6465	0.1197	3.9286	0.1165
Average (m)	0.1689	0.1219	0.1187	3.6378	0.1219	3.9315	0.1185
Stanard (std)	0.003148	0.004367	0.003986	0.009936	0.004626	0.005385	0.004161

6.4. Pattern recognition with Hamming network

As shown in Fig. 19, the feedforward layer calculates the inner product between each representative pattern and the current pattern. The value of each of the seven characteristic parameters corresponding to ten representative patterns is transformed into the binary form and stored in the weight matrix $\mathbf{W^1}$. The ten neurons storing the results of the inner product in the feedforward layer compete with each other to determine a winner. After the competition, only one neuron will have a non-zero output, and this neuron indicates the representative pattern that is closest to a current pattern.

6.5. Verification

The DCIR results for the ten representative batteries were compared with an unknown pattern, as shown in Table 6, and the outputs of the two layers of the Hamming network for three

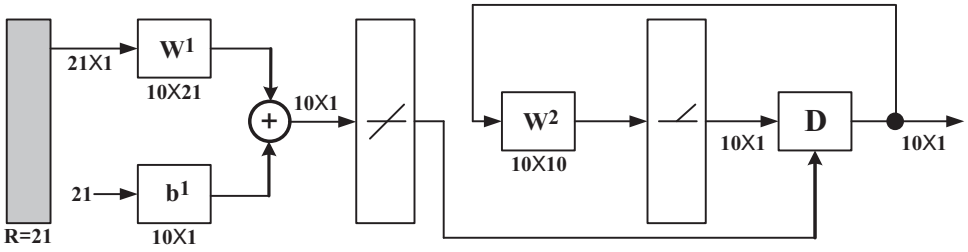

Fig. 19. Hamming network used in the study.

Table 6
DCIR results of ten Li-ion batteries used as representatives [Ω].

Battery	SoC								
	10%	20%	30%	40%	50%	60%	70%	80%	90%
No. 1	0.07431	0.07424	0.07248	0.07137	0.07018	0.07270	0.07397	0.07259	0.07138
No. 2	0.07999	0.07719	0.07628	0.07375	0.07239	0.07486	0.07688	0.07571	0.07576
No. 3	0.08077	0.07787	0.07656	0.07450	0.07278	0.07550	0.07762	0.07656	0.07645
No. 4	0.08183	0.07922	0.07796	0.07709	0.07607	0.07883	0.07916	0.07800	0.07717
No. 5	0.07449	0.07329	0.07240	0.07125	0.07029	0.07303	0.07361	0.07333	0.07200
No. 6	0.07832	0.07609	0.07494	0.07264	0.07164	0.07353	0.07508	0.07425	0.07423
No. 7	0.08503	0.08146	0.08059	0.07962	0.07844	0.08108	0.08153	0.08035	0.07889
No. 8	0.07257	0.07140	0.07005	0.06879	0.06769	0.07018	0.07076	0.07036	0.07012
No. 9	0.07179	0.06969	0.06878	0.06725	0.06569	0.06876	0.06948	0.06921	0.06926
No. 10	0.07519	0.07369	0.07302	0.07151	0.06963	0.07328	0.07404	0.07308	0.07270

unknown patterns are shown in Figs. 20–22. In each case, it seen that, in the recurrent layer only the selected representative pattern has a non-zero output. In addition, as demonstrated in Table 7, the DCIR results of the three unknown batteries are similar to those of the representative pattern selected.

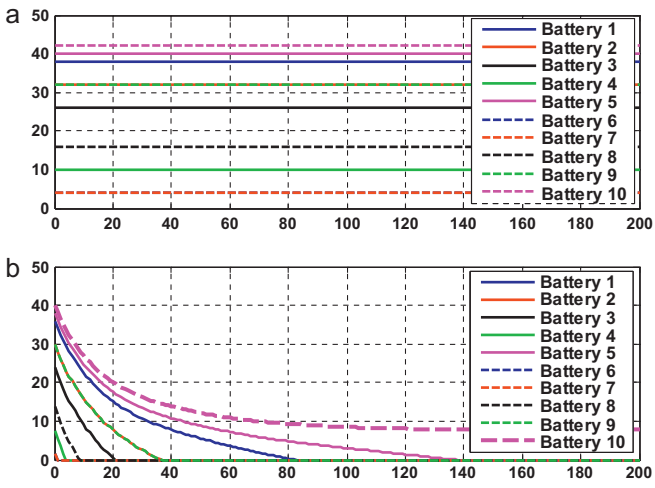

Fig. 20. Outputs of two neural network layers (arbitrary battery 1, selected pattern No. 10): (a) feedforward layer; (b) recurrent layer.

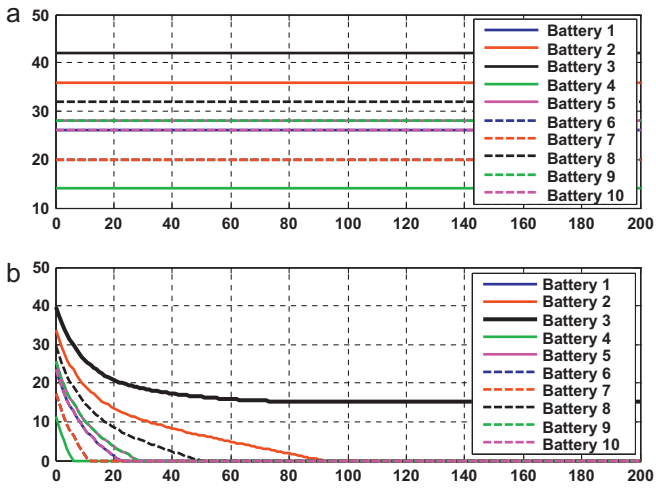

Fig. 21. Outputs of two neural network layers (arbitrary battery 2, selected pattern No. 3): (a) feedforward layer; (b) recurrent layer.

6.6. SoC estimation

In the proposed method, as shown in Fig. 1, the OCV, R_i, R_{Diff}, C_{Diff}, and capacity are measured in advance. For reference, it is assumed that R_i is constant, R_{Diff}/C_{Diff} is the time constant τ (= 46.37 s), and SoC is 50%. The OCVs and other model parameters are listed in Fig. 23 and Table 8, respectively.

Table 7
DCIR results of three unknown Li-ion batteries [Ω].

Battery	SoC								
	10%	20%	30%	40%	50%	60%	70%	80%	90%
Test 1	0.07552	0.07381	0.07330	0.07173	0.06978	0.07341	0.07411	0.07316	0.07283
Test 2	0.08068	0.07775	0.07642	0.07431	0.07256	0.07533	0.07787	0.07665	0.07654
Test 3	0.07453	0.07412	0.07235	0.07123	0.07032	0.07252	0.07387	0.07243	0.07131

Table 8
Model parameters of ten Li-ion batteries used as representatives.

Battery	SoC		
	Diffusion resistance R_{Diff} [Ω]	Diffusion capacitance C_{Diff} [F]	Capacity [Ah]
No. 1	0.02918	1589.19	1.2748
No. 2	0.03139	1477.30	1.2844
No. 3	0.03178	1459.17	1.2826
No. 4	0.03507	1322.28	1.2841
No. 5	0.02929	1583.22	1.2865
No. 6	0.03064	1513.46	1.2761
No. 7	0.03764	1238.58	1.2925
No. 8	0.02669	1737.45	1.2753
No. 9	0.02469	1878.19	1.2704
No. 10	0.02863	1619.72	1.2796

R_i = 0.04110 Ω, τ = 46.37 s

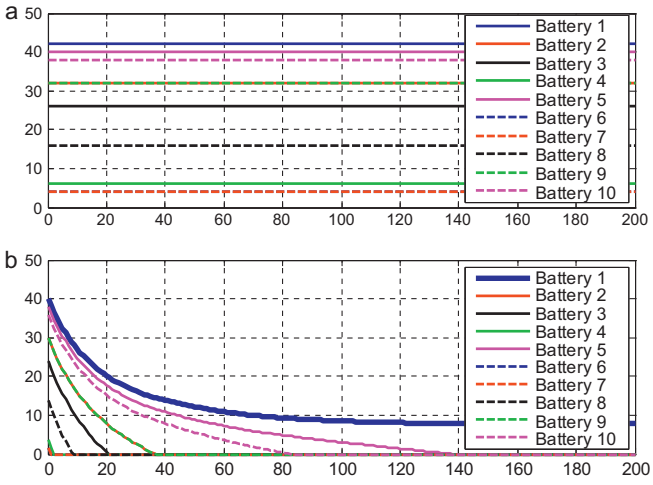

Fig. 22. Outputs of two neural network layers (arbitrary battery 3, selected pattern No. 1): (a) feedforward layer; (b) recurrent layer.

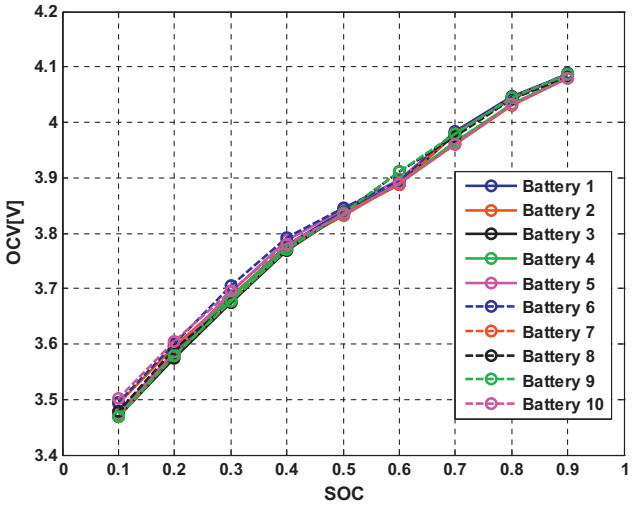

Fig. 23. Open circuit voltages (OCV) of ten Li-ion batteries.

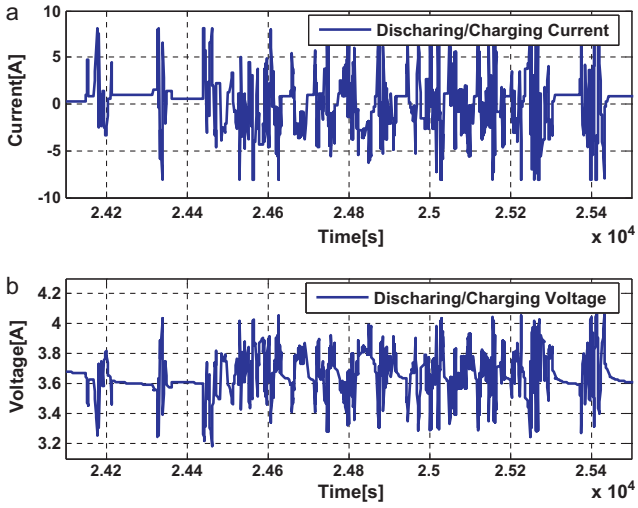

Fig. 24. Two plots for discharging/charging of unknown battery: (a) current profile; (b) voltage data.

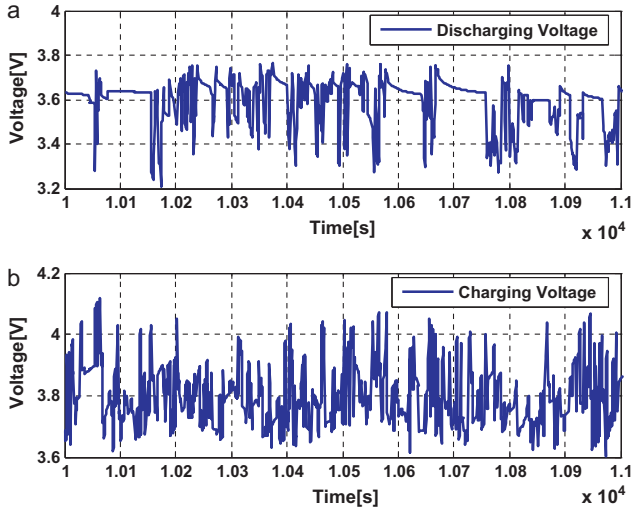

Fig. 25. Two separated voltages from discharging/charging voltage of arbitrary battery: (a) discharging voltage; (b) charging voltage.

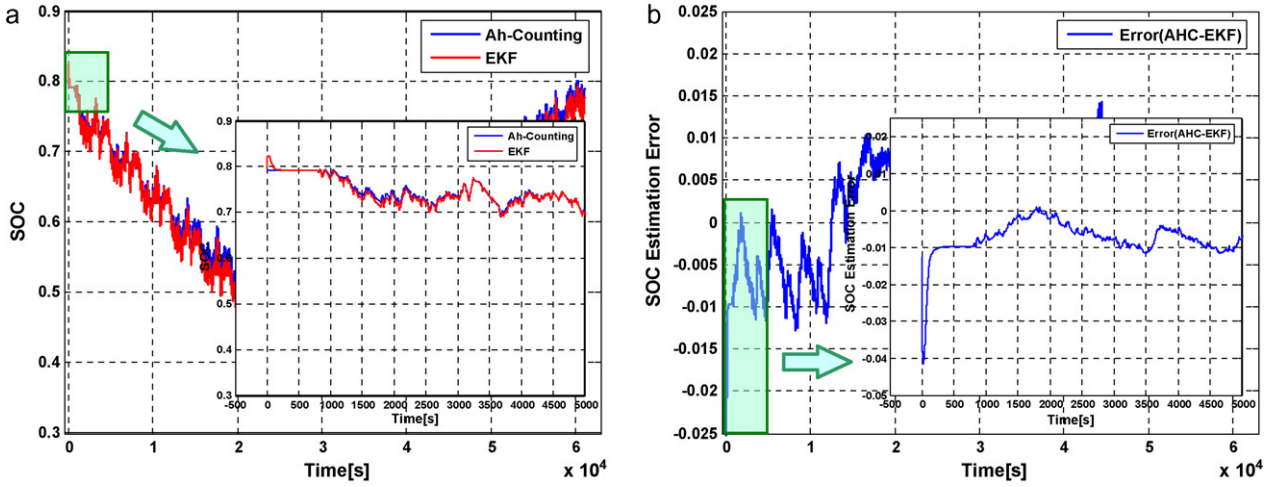

Fig. 26. SoC estimation based on EKF in comparison with ampere-hour counting (arbitrary battery 1, selected pattern No. 10): (a) SoC estimation (initial SoC 79.85%); (b) estimation error.

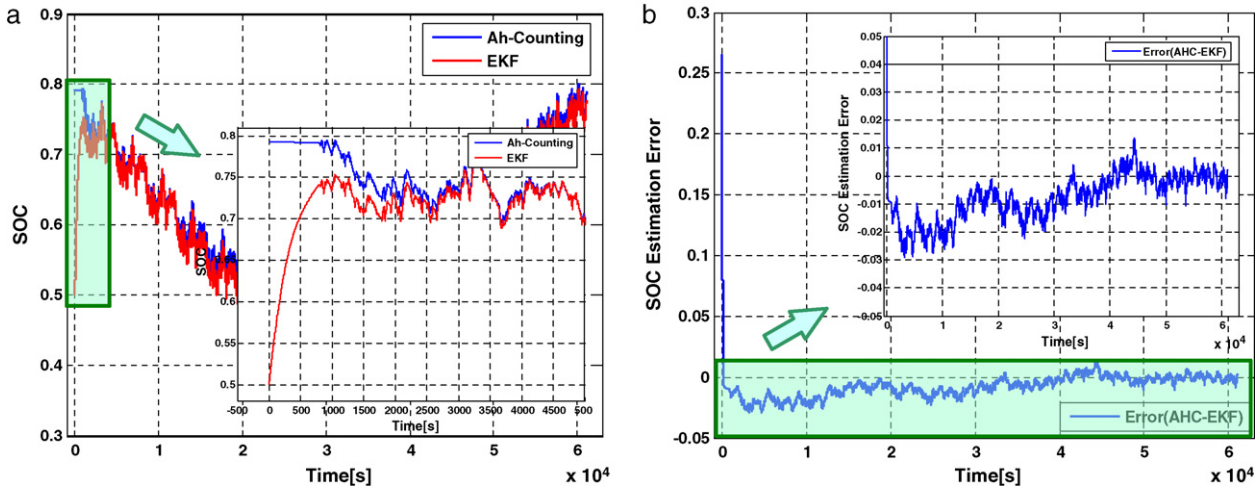

Fig. 27. SoC estimation based on EKF in comparison with ampere-hour counting (arbitrary battery 2, selected pattern No. 3): (a) SoC estimation (initial SoC 0.5); (b) estimation error.

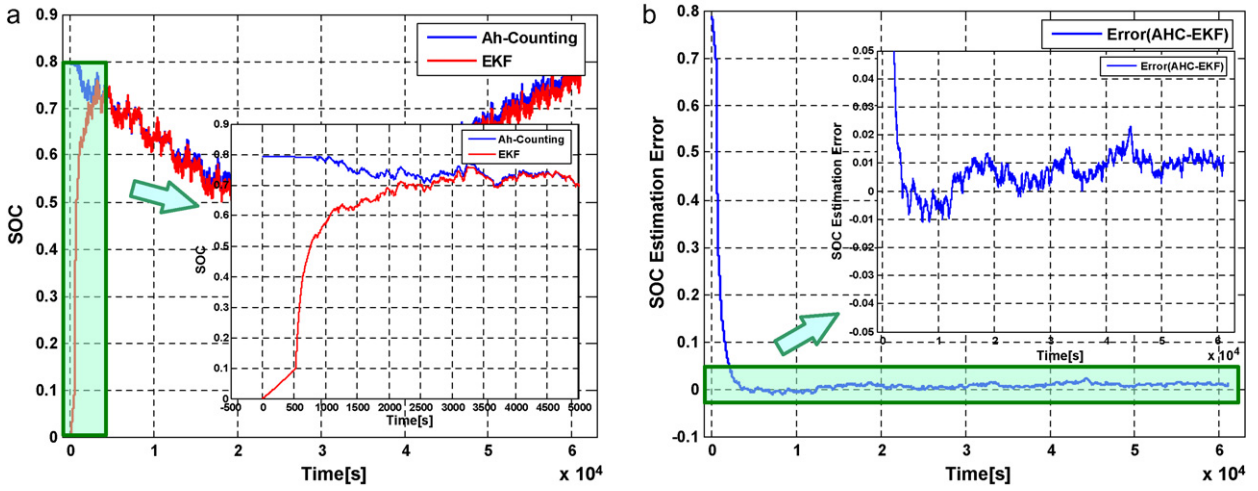

Fig. 28. SoC estimation based on EKF in comparison with ampere-hour counting (arbitrary battery 3, selected pattern No. 1): (a) SoC estimation (initial SoC 0); (b) estimation error.

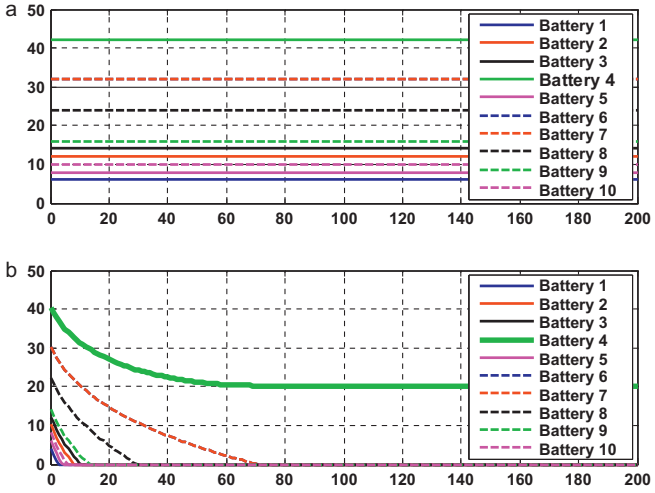

Fig. 29. Outputs of two layers (arbitrary battery, selected pattern No. 4): (a) feed-forward layer; (b) recurrent layer.

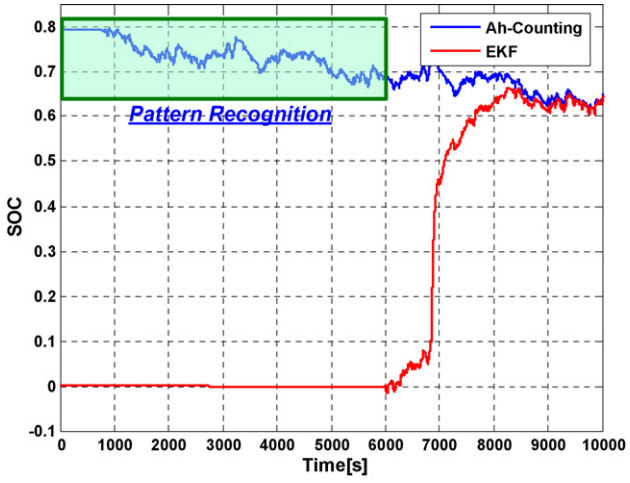

Fig. 30. Online SoC estimation based on EKF in comparison with ampere-hour counting (arbitrary battery, selected pattern No. 4).

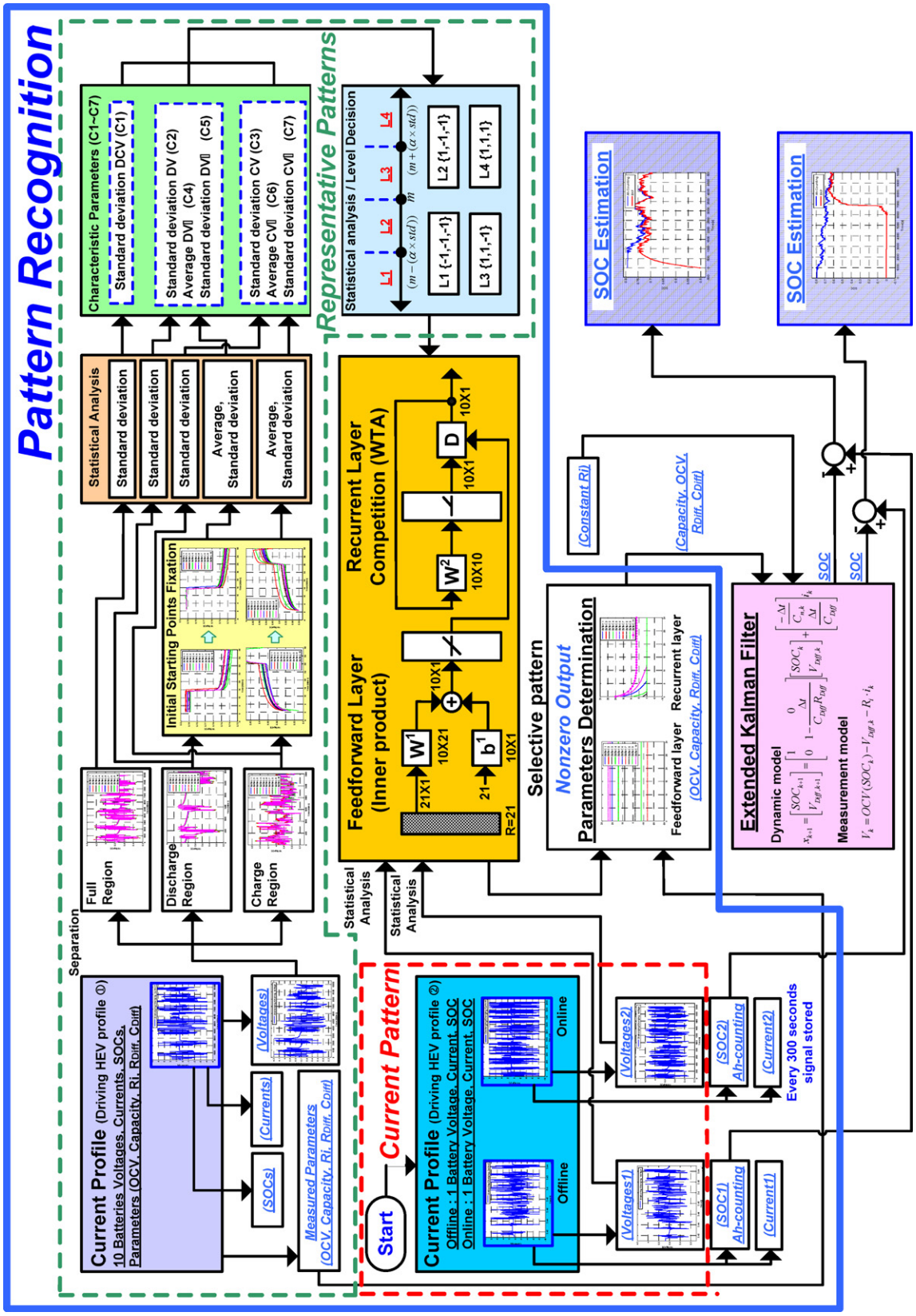

Fig. 31. Schematic diagram of proposed method.

Table 9
DCIR results for unknown Li-ion battery used for online SoC estimation [Ω].

Battery	SoC								
	10%	20%	30%	40%	50%	60%	70%	80%	90%
Test 1	0.08212	0.07981	0.07852	0.07773	0.07645	0.07921	0.07974	0.07789	0.07701

6.6.1. Off-line SoC estimation

As shown in Fig. 24(a), another scaled-down HEV automotive current profile (time interval, 1 s) was applied to the battery to be measured. Then, as seen in Fig. 24(b), the discharging/charging voltage data were collected. Then the discharging/charging voltage was separated into the discharging and charging voltage, as presented in Fig. 25. Next, for the three unknown batteries in Section 6.5, the model parameters of selected representative patterns were used to estimate the SoC. Thus, it is possible to estimate the SoC for an arbitrary battery, without the need for repeated measurement of model parameters. As indicated in Figs. 26–28, all SoC estimates were within ±5% of the ampere-counting results.

6.6.2. On-line SoC estimation

Offline SoC estimation involves sequential processing. After discharging–charging a battery using a scaled HEV driving current profile, pattern recognition and SoC estimation were performed sequentially. This off-line processing is very useful to screen the batteries that have similar electrochemical characteristics under discharging/charging during a long period time over a fully SoC range, because it cannot be assured that discharging/charging during a short period time can determine the electrochemical characteristic of a battery [51]. For SoC estimation, however, it may be time-consuming. The proposed method relies on constant model parameters for a set of selected representative patterns for SoC estimation. Therefore, in order to reduce the SoC estimation error in comparison with off-line processing, online SoC estimation can be performed. The same discharging/charging current profile as that used for off-line SoC estimation is adopted. During discharging/charging, only voltage data for the last 6000 s are necessary for pattern recognition. Every 300 s, the stored signals are analyzed statistically. The storing period of signals, i.e., 1 s, and the updating period of the control algorithm, 300 s, were selected so as not overload the control unit. Then, the SoC estimation is not absolutely performed during this period. After pattern recognition, the model parameters of the selected battery are used to estimate the SoC. As shown in Fig. 29, the selected representative pattern is No. 4. The DCIR for the unknown battery is compared with that of representative pattern of No. 4 in Table 9. As shown in Fig. 30, the estimated SoC using the parameters of representative battery No. 4 are within ±5% of the estimated obtained by ampere-hour counting. A schematic diagram of the proposed method is given in Fig. 31.

7. Conclusion

Precise SoC estimation is critical for practical applications and to prevent over-charging and over-discharging of Li-ion batteries that may cause permanent internal damage. Unfortunately, however, the existing EKF algorithm does not account for variations in battery parameters due to differences in electrochemical characteristics and the effects of temperature and ageing. This study proposes a method to identify the characteristics of Li-ion batteries using the Hamming network for improved SoC estimation. The discharging/charging voltage patterns of ten fresh representative Li-ion batteries are used. The model parameters of a representative battery that most closely matches the discharging/charging voltage pattern of the unknown battery to be measured are used for SoC estimation by the conventional EKF. This avoids the need for measurement of battery parameters before every SoC estimation process. It can be concluded that SoC estimation can be selectively and quickly implemented off-line or on-line by the proposed methods for discharging/charging a battery in, for example, screening processes. The proposed method produces estimates that are within ±5% of those obtained by ampere-hour counting.

Acknowledgement

This work was supported by the ERC program of MOST/KOSEF (Grant No. R11-2002-102-00000-0).

References

[1] H.-S. Park, C.-E. Kim, C.-H. Kim, G.-W. Moon, J.-H. Lee, IEEE Trans. Ind. Electron. 56 (5) (2009) 1464–1476.
[2] H.-S. Park, C.-E. Kim, C.-H. Kim, G.-W. Moon, J.-H. Lee, J. Power Electron. 9 (3) (2007) 343–352.
[3] Y.-S. Lee, W.-Y. Wang, T.-Y. Kuo, IEEE Trans. Ind. Electron. 55 (1) (2008) 218–228.
[4] S.M. Lukic, J. Cao, R.C. Bansal, F. Rodriguez, A. Emadi, IEEE Trans. Ind. Electron. 55 (6) (2008), 2558-2267.
[5] M. Coleman, C.K. Lee, C. Zhu, W.G. Hurley, IEEE Trans. Ind. Electron. 54 (5) (2007) 2550–2557.
[6] J. Wang, B. Cao, Q. Chen, F. Wang, Control Eng. Pract. 15 (12) (2007) 1569–1576.
[7] I. Snihir, W. Rey, E. Verbitskiy, A. Belfadhel-Ayeb, P.H.L. Notten, J. Power Sources 159 (2006) 1484–1487.
[8] T. Hansen, C.-J. Wang, J. Power Sources 141 (2005) 351–358.
[9] N. Abolhassani Monfared, N. Gharib, H. Moqtaderi, M. Hejabi, M. Amiri, F. Torabi, A. Mosahebi, J. Power Sources 158 (2006) 932–935.
[10] A.J. Salkind, C. Fennie, P. Singh, T. Atwater, D.E. Reisner, J. Power Sources 80 (1999) 293–300.
[11] G.L. Plett, J. Power Sources 134 (2004) 252–292.
[12] V. Vasebi, M. Partovibakhsh, M.T. Bathaee, J. Power Sources 174 (2007) 30–40.
[13] J. Han, D. Kim, M. Sunwoo, J. Power Sources 188 (2009) 606–612.
[14] J.-S. Koo, S.-S. Park, K.-Y. Youn, C.-S. Kim, Development of SoC Estimation Logic Using the Steady State DC-IR for SHEV, in: Electric Vehicle Symposium, 2001.
[15] S.J. Lee, J.H. Kim, J.M. Lee, B.H. Cho, The Maximum Pulse Current Estimation for the Lithium-Ion Battery, in: IEEE Applied Power Electronics Conference and Exposition, 2008.
[16] O. Nam, J. Lee, J. Lee, J. Kim, B.H. Cho, Li-Ion Battery SoC Estimation Method based on the Reduced Order Extended Kalman Filtering, in: IEEE International Energy Conversion Engineering Conference, 2006.
[17] S. Lee, J. Kim, J. Lee, J. Power Sources 185 (2008) 1367–1373.
[18] J. Lee, O. Nam, B.H. Cho, J. Power Sources 174 (2007) 9–15.
[19] J.P. Christophersen, G.L. Hunt, C.D. Ho, D. Howell, J. Power Sources 173 (2007) 998–1005.
[20] J. Shim, K.A. Striebel, J. Power Sources 122 (2003) 188–194.
[21] K. Kato, A. Negishi, K. Nozaki, I. Tsuda, K. Takano, J. Power Sources 117 (2003) 118–123.
[22] M.D. Levi, C. Wang, D. Aurbach, Z. Chvoj, J. Electroanal. Chem. 562 (2004) 187–203.
[23] P. Ramadass, B. Haran, R. White, B.N. Popov, J. Power Sources 112 (2002) 606–613.
[24] M. Kerlau, R. Kostechi, J. Electrochem. Soc. 153 (2006) A1644–A1648.
[25] P. Suresh, A.K. Shukla, N. Munichandraiah, J. Appl. Electrochem. 32 (2002) 267–273.
[26] J.R. Belt, C.D. Ho, J. Ted, M. Miller, A. Habib, T.Q. Duong, J. Power Sources 142 (2005) 354–360.
[27] V.H. Johnson, A.A. Pesaran, T. Sack, Temperature Dependent Battery Models for High-Power Lithium-Ion Batteries, in: Electric Vehicle Symposium, 2000.
[28] E.P. Roth, D.H. Doughty, J. Power Sources 128 (2004) 308–318.
[29] K. Onda, T. Ohshima, M. Nakayama, K. Fukuda, T. Araki, J. Power Sources 158 (2006) 535–542.
[30] D.H. Doughty, E.P. Roth, C.C. Crafts, G. Nagasubramanian, G Henriksen, K Amine, J. Power Sources 146 (2005) 116–120.
[31] J. Kim, S. Lee, B. Cho, The State of Charge Estimation Employing Empirical Parameters Measurements for Various Temperatures, in: IEEE International Power Electronics and Motion Control Conference, 2006.

[32] E.V. Thomas, H.L. Case, D.H. Doughty, R.G. Jungst, G. Nagasubramanian, E.P. Roth, J. Power Sources 124 (2003) 254–260.
[33] J. Vetter, P. Novák, M.R. Wagner, C. Veit, K.-C. Möller, J.O. Besenhard, M. Winter, M. Wohlfahrt-Mehrens, C. Vogler, A. Hammouche, J. Power Sources 147 (2005) 269–281.
[34] M. Broussely, S. Herreyre, P. Biensan, P. Kasztejna, K. Nechev, R.J. Staniewicz, J. Power Sources 97–98 (2001) 13–21.
[35] M. Wohlfahrt-Mehrens, C. Vogler, J. Garche, J. Power Sources 127 (2004) 58–64.
[36] U. Tröltzsch, O. Kanoun, H.-R. Tränkler, Electrochim. Acta 51 (2006) 1664–1672.
[37] R.B. Wright, J.P. Christophersen, C.G. Motloch, J.R. Belt, C.D. Ho, V.S. Battaglia, J.A. Barnes, T.Q. Duong, R.A. Sutula, J. Power Sources 119–121 (2003) 865–869.
[38] M. Broussely, Ph. Biensan, F. Bonhomme, Ph. Blanchard, S. Herreyre, K. Nechev, R.J. Staniewicz, J. Power Sources 146 (2005) 90–96.
[39] C.C. Bloom, S.A. Jones, V.S. Battaglia, G.L. Henriksen, J.P. Christophersen, R.B. Wright, C.D. Ho, J.R. Belt, C.G. Motloch, J. Power Sources 124 (2003) 538–550.
[40] D.P. Abraham, J. Liu, C.H. Chen, Y.E. Hyung, M. Stoll, N. Elsen, S. MacLaren, R. Twesten, R. Haasch, E. Sammann, I. Petrov, K. Amine, G. Henriksen, J. Power Sources 119–121 (2003) 511–516.
[41] M.-S. Wu, P.-C.J. Chiang, J.-C. Lin, J. Electrochem. Soc. 152 (2005) A1041–A1046.
[42] J.H. Kim, S.J. Lee, J.M. Lee, B.H. Cho, A New Direct Current Internal Resistance and State of Charge Relationship for the Li-Ion Battery Pulse Power Estimation, in: IEEE International Conference on Power Electronics, 2007.
[43] R.B. Wright, C.G. Motloch, Calendar-Life Studies of Advanced Technology Development Program Gen 1 Lithium Ion Batteries, U.S. Department of Energy, 2001.
[44] K. Koutroumbas, N. Kalouptsidis, Neural Netw. 18 (7) (2005) 896–913.
[45] J.G. Guimarães, L.M. Nóbrega, J.C. da Costa, Microelectron. J. 37 (6) (2006) 510–518.
[46] I. Meilijon, E. Ruppin, M. Sipper, IEEE Trans. Neural Netw. 6 (1) (1995) 261–266.
[47] L. Chen, N. Tokuda, A. Nagaim, Neural Netw. 20 (5) (2007) 598–609.
[48] J.-C. Chang, IEEE Trans. Inf. Theory 52 (4) (2006) 1683–1689.
[49] S.P. Perone, W.C. Spindler, J. Power Sources 13 (1984) 23–38.
[50] M.T. Hagan, H.B. Demuth, M. Beale, Neural Network Design, first ed., PWS Publishing Co., Boston, MA, 1995.
[51] J.-H. Kim, J.-W. Shin, C.-Y. Jeon, B.-H. Cho, Screening Process of Li-Ion Series Battery Pack for Improved Voltage/SoC Balancing, in: IEEE International Power Electronics Conference, 2010.